

Pyrrolopyridine Inhibitors of Mitogen-Activated Protein Kinase-Activated Protein Kinase 2 (MK-2)

David R. Anderson,* Marvin J. Meyers,* William F. Vernier, Matthew W. Mahoney, Ravi G. Kurumbail, Nicole Caspers, Gennadiy I. Poda, John F. Schindler, David B. Reitz, and Robert J. Mourey

Pfizer Global Research and Development, St. Louis Laboratories, 700 Chesterfield Parkway W, Chesterfield, Missouri 63017

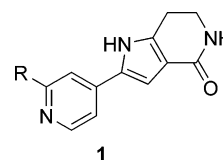
Received September 20, 2006

A new class of potent kinase inhibitors selective for mitogen-activated protein kinase-activated protein kinase 2 (MAPKAP-K2 or MK-2) for the treatment of rheumatoid arthritis has been prepared and evaluated. These inhibitors have IC₅₀ values as low as 10 nM against the target and have good selectivity profiles against a number of kinases including CDK2, ERK, JNK, and p38. These MK-2 inhibitors have been shown to suppress TNF α production in U397 cells and to be efficacious in an acute inflammation model. The structure–activity relationships of this series, the selectivity for MK-2 and their activity in both in vitro and in vivo models are discussed. The observed selectivity is discussed with the aid of an MK-2/inhibitor crystal structure.

Introduction

Tumor necrosis factor- α (TNF α) is a cytokine that is overproduced in inflammatory disease states such as rheumatoid arthritis (RA).¹ Clinical efficacy and FDA approval of anti-TNF α biologics such as etanercept, infliximab, and adalimumab demonstrate the importance of TNF α in inflammatory disease.^{2–5} Similarly, small molecule inhibitors of TNF α production would be expected to be effective as disease modifying treatments for RA and other inflammatory diseases. A number of potential biological targets for inhibition of TNF α biosynthesis have been identified. Inhibitors of p38 MAP kinase have been shown to play an important role in the regulation of the production of inflammatory cytokines such as TNF α .^{6,7} Furthermore, p38 MAP kinase inhibitors have been shown to be efficacious in RA patients in clinical trials. For example, VX-745 demonstrated efficacy in a 12-week clinical study,⁸ but development was suspended due to adverse CNS effects observed at high doses in animal models.⁹ More recently, VX-702 was reported as being efficacious for the treatment of RA in a phase II trial in combination with methotrexate.¹⁰

Mitogen-activated protein kinase-activated protein kinase-2 (MAPKAP-K2 or MK-2) is a direct substrate of p38 and regulates cytokine production through a post-transcriptional mechanism.^{11–13} MK-2 knockout mice express TNF α when challenged with lipopolysaccharide (LPS), but only to about 10–20% of the levels expressed by wild-type mice.¹¹ Importantly, while MK-2 knockout mice are healthy and have a normal phenotype, deletion of the p38 α gene is embryonic lethal. In addition, MK-2 knockout mice have been shown to be resistant to developing arthritis in animal models.¹⁴ These observations suggest that a selective MK-2 inhibitor may demonstrate efficacy equal to that of a p38 inhibitor without affecting additional cellular pathways governed by p38 that may lead to undesirable side effects. In this report, we disclose the preparation of a series of potent, selective inhibitors of MK-2 and their effectiveness in blocking the production of TNF α . These compounds have the general structure shown in **1**.



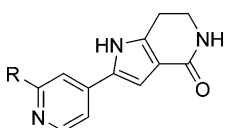
Results and Discussion

Chemistry. This series of compounds, originating from modification of a hit obtained from high-throughput screening, can be made via the general synthesis of compounds as shown in Scheme 1. Commercially available 2-chloro-4-cyanopyridine **2** was converted to the methyl ketone **3** by treatment with methylmagnesium bromide followed by hydrolysis.¹⁵ Ketone **3** was brominated with bromine and HBr to give bromoketone **4**. Bromoketones **4** and **5** (commercially available) were reacted with piperidine-2,4-dione (**6**) and ammonium acetate to generate pyrroles **7** and **8** via a one-pot three-component pyrrole condensation reaction. Chloropyridine **7** was readily scaled and served as a useful late-stage intermediate for rapid analog preparation. Facile Suzuki coupling of aromatic and heteroaromatic boronic acids or their pinacol esters to **7** allowed access to a variety of analogs in short order using solution-phase parallel synthesis techniques.

To broaden the scope of the structure–activity relationships (SAR), a variety of amides (**32–37**) were prepared. The amides were either prepared via Suzuki coupling of the corresponding commercially available boronic acids to chloropyridine **7** (Scheme 1) or by amide bond coupling to carboxylic acid **31** (Scheme 2).

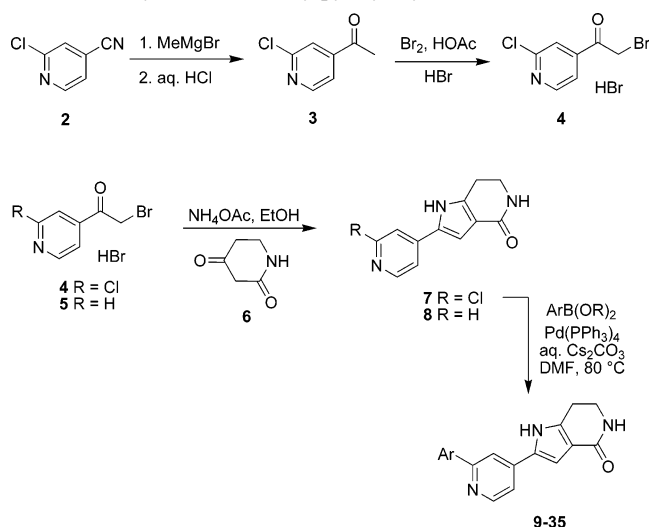
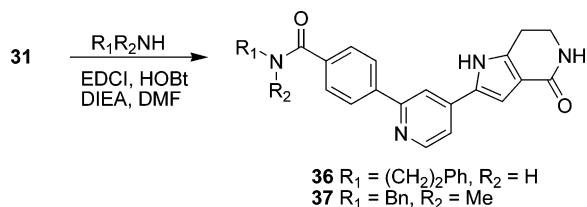
In Vitro Potency and Selectivity. Tables 1 and 2 summarize the in vitro potency found in this series of compounds. The inhibitors discovered were found to be competitive with ATP. Increasing ATP concentrations in the enzyme assay to levels above the K_m for MK-2 (30 μ M) induced a right shift in the apparent IC₅₀ to higher values. Detailed kinetic analysis of compound **23**, for example, showed a classic ATP competitive mechanism in a Lineweaver–Burke plot of the data (see Supporting Information Figure S1). Most compounds prepared showed good potency against the isolated MK-2 enzyme while exhibiting some SAR trends. The unadorned phenyl ring (**9**) provided improved potency relative to H (**8**) or Cl (**7**; Table 1). In fact, a wide variety of aryl and heteroaryl rings (**9–16**) were

* To whom correspondence should be addressed. Phone: 636-247-7651 (D.R.A.); 636-247-7672 (M.J.M.). Fax: 636-247-5400 (D.R.A.); 636-247-6953 (M.J.M.). E-mail: david.r.anderson@pfizer.com (D.R.A.); marvin.j.meyers@pfizer.com (M.J.M.).

Table 1. Inhibition of MK-2 and TNF α Production in U937 Cells by 2-Aryl Pyridine Analogs


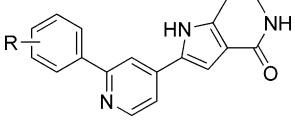
compd	R	MK-2 IC ₅₀ ^a (μ M)	U937 IC ₅₀ ^b (μ M)
8	H	0.171 \pm 0.082	19
7	Cl	0.608 \pm 0.263	
9	Ph	0.066 \pm 0.029	1.4
10	4-pyridine	0.056 \pm 0.026	23
11	3-pyridine	0.048 \pm 0.005	9.9
12	5-pyrimidine	0.083 \pm 0.026	>100
13	3-thienyl	0.076 \pm 0.020	6.8
14	3-naphthyl	0.052 \pm 0.012	4.2
15	2-benzothienyl	0.030 \pm 0.0001	5.7
16	3-quinoline	0.0085 \pm 0.0016	4.4

^a Values are reported as the mean \pm standard deviation ($n \geq 2$). ^b IC₅₀ values are reported as the mean of 2–3 experiments with a standard deviation less than 3-fold.

Scheme 1. Synthesis of 2-Arylpyridyl Pyrroles**Scheme 2.** Synthesis of Aryl Amides

not only tolerated, but enhanced enzyme potency. The 3-quinoline substitution (**16**) represents one of the most potent compounds identified in this series.

A wide variety of substituents were tolerated on the phenyl ring as well (Table 2). In general, ortho substituents were poorly tolerated (**17**, **20**, **23**), while both meta (**18**, **21**, **24**) and para (**19**, **22**, **25**) substitutions were preferred. This suggests that the dihedral angle between the pyridine and the aryl ring may be important for potency. The enzyme is also quite tolerant of a diverse array of substituents, regardless of size or electron-donating or electron-withdrawing character (**26–31**), which had little effect on measured potencies. Additionally, a variety of secondary amides were found to be especially potent MK-2 inhibitors (**32–37**). There is, however, a limit to the size of the

Table 2. Inhibition of MK-2 and TNF α Production in U937 Cells by 2-Aryl Pyridine Analogs


compd	R	MK-2 IC ₅₀ ^a (μ M)	U937 IC ₅₀ ^b (μ M)
17	2-OH	0.410 \pm 0.058	47
18	3-OH	0.025 \pm 0.012	36
19	4-OH	0.021 \pm 0.001	35
20	2-Cl	0.606 \pm 0.004	9.0
21	3-Cl	0.037 \pm 0.003	4.6
22	4-Cl	0.032 \pm 0.006	2.7
23	2-F	0.126 \pm 0.038	4.8
24	3-F	0.030 \pm 0.005	7.4
25	4-F	0.050 \pm 0.030	2.4
26	4-CF ₃	0.071 \pm 0.0004	3.8
27	4-CN	0.062 \pm 0.013	>100
28	4-Ac	0.051 \pm 0.009	18
29	4-MeO	0.055 \pm 0.015	2.2
30	4-NH ₂	0.041 \pm 0.007	12
31	4-CO ₂ H	0.022 \pm 0.006	>100
32	4-CONH- <i>c</i> -Pr	0.015 \pm 0.003	>100
33	4-CONH- <i>c</i> -pentyl	0.008 \pm 0.002	23
34	4-CONH- <i>c</i> -Hex	0.017 \pm 0.007	10
35	4-CONHCH ₂ Ph	0.008 \pm 0.003	20
36	4-CONH(CH ₂) ₂ Ph	0.046 \pm 0.005	11
37	4-CON(Me)CH ₂ Ph	0.056 \pm 0.004	15

^a Values are reported as the mean \pm standard deviation ($n \geq 2$). ^b IC₅₀ values are reported as the mean of 2–3 experiments with a standard deviation less than 3-fold.

Table 3. Kinase Selectivity of Potent MK-2 Inhibitors

compd	8	9	16	23
aryl group	H	Ph	3-quinolinyl	2-F-Ph
kinase IC ₅₀ ^a (μ M)				
MK-2	0.171	0.066	0.0085	0.126
MK-3	57.7	0.66	0.21	1.1
PRAK (MK-5)	0.50	0.14	0.081	0.21
MNK1	2.67	16	5.7	>10
MSK1	2.34	146	>200	>200
MSK2	3.01	148	>200	58
CDK2	0.17	18	>200	30
ERK2			3.44	4.6
JNK2			>200	21
IKK2	>10	>200	>200	>200
p38a			>100	87

^a IC₅₀ values are reported as the mean of 2–3 experiments with a standard deviation of less than 3-fold.

amide, as demonstrated by **36**. Tertiary amides (**37**) were somewhat less potent than secondary amides (**35**).

Selectivity against other related MAPKAP kinases, CDK2, and kinases associated with TNF α production for several of the more potent analogs is recorded in Table 3. To utilize IC₅₀ values to compare the selectivity of compounds between kinase assays, K_m values for ATP with each kinase was determined and all kinase selectivity reactions were run at K_m values of ATP (see Supporting Information). While the unsubstituted analog (**8**) had no selectivity against CDK2, most 2-aryl substituted compounds (e.g., **9**, **16**, and **23**) demonstrated exceptional selectivity against CDK2, ERK2, JNK2, IKK2, as well as MNK1, MSK1, and MSK2. The MAPKAP kinases MK-3, PRAK (MK-5), MNK1, MSK1, and MSK2 are all direct substrates of p38, with MK-3 and PRAK sharing the highest degree of sequence identity with MK-2. Therefore, it is not surprising that most compounds show only modest selectivity versus PRAK and MK-3. The fact that this series of compounds shows some selectivity against these related kinases is indeed

noteworthy. Importantly, these selected compounds show little activity on any pathway known to be implicated in TNF α production (e.g., p38 α , ERK2, JNK2, and IKK2) except for their inhibition of MK-2 or its close homologues, MK-3 and PRAK.

Crystallography and Rationale for Selectivity. To understand the details of the molecular interactions of MK-2 inhibitors with protein kinases, we undertook crystallographic analysis of the inhibitors complexed with MK-2 and CDK2. Prior to the availability of these crystal structures, we had obtained the structure of MK-2 complexed with AMPPNP, a nonhydrolyzable analog of ATP.¹⁶ Docking studies of early lead compounds into the MK-2 crystal structure suggested that substitution at the 2-position of the pyridyl group could potentially enhance the potency of these compounds for MK-2. Moreover, an overlay of MK-2 and CDK2 crystal structures revealed two key structural differences between these two kinases: (1) the presence of a large hydrophobic pocket in MK-2 in the hinge region of the ATP site due to the presence of an additional amino acid relative to CDK2 and (2) substitution of a key tyrosine residue in the hinge region of CDK2 by a smaller cysteine residue in MK-2. The latter results in a more expanded pocket in MK-2 near the protein surface. We hypothesized that analogues containing large, rigid groups from the 2-position of the pyridyl moiety of our inhibitors could have decreased binding affinity for CDK2 relative to MK-2 because of the above structural features.

A crystal structure of compound **23** complexed with MK-2 was determined at 3.8 Å resolution (Figure 1a,b). Although the modest resolution of the crystal structure prevents us from making definite conclusions regarding hydrogen bonds and other intermolecular interactions, the pyridyl nitrogen of the inhibitor is within a reasonable distance (3.4 Å) of forming a hydrogen bond with the peptide nitrogen of Leu141. The lactam moiety appears to form two hydrogen bonds in the phosphate binding region of MK-2. While the oxygen of lactam forms a hydrogen bond to the terminal nitrogen of the conserved lysine (Lys93), the lactam nitrogen engages the side chain carboxylate of the conserved aspartic acid, Asp207. In addition, the ligand forms close van der Waals interactions with several protein residues in the active site including the gatekeeper residue, Met138. Clear electron density is visible for most of the glycine-rich loop, which is a relatively flexible segment in many protein kinase structures. The 2-fluorophenyl group of the inhibitor is sandwiched between the glycine loop and the hinge region of MK-2, with good lipophilic interactions with the side chain of Leu70 of the glycine loop. The fluorine atom is located near the side chain of Leu193 of the carboxy-terminal domain of MK-2. The terminal aryl group of the ligand is rotated by ~37 degrees relative to the rest of the inhibitor.

Superposition of the crystal structure of CDK2 on the MK-2 structure reveals the structural basis for the specificity of the aryl analogues of the pyrrole lactam series of inhibitors (Figure 1c). As shown in Table 3, compounds that contain large aromatic substituents from the 2-position of the pyridyl moiety are highly selective for MK-2, MK-3, and PRAK compared to other kinases. The side chain of Cys140 is located near the terminal aryl group of compound **23** in the crystal structure. Most kinases possess an amino acid with a large side chain at a position corresponding to Cys140 of MK-2. It is very likely that the presence of bulky side chains in these kinases could form a steric clash with the terminal aryl group of compound **23** and related analogues. In fact, there are only eight other kinases in the entire human kinome that contain a cysteine or a smaller amino acid at a position corresponding to Cys140 of MK-2.

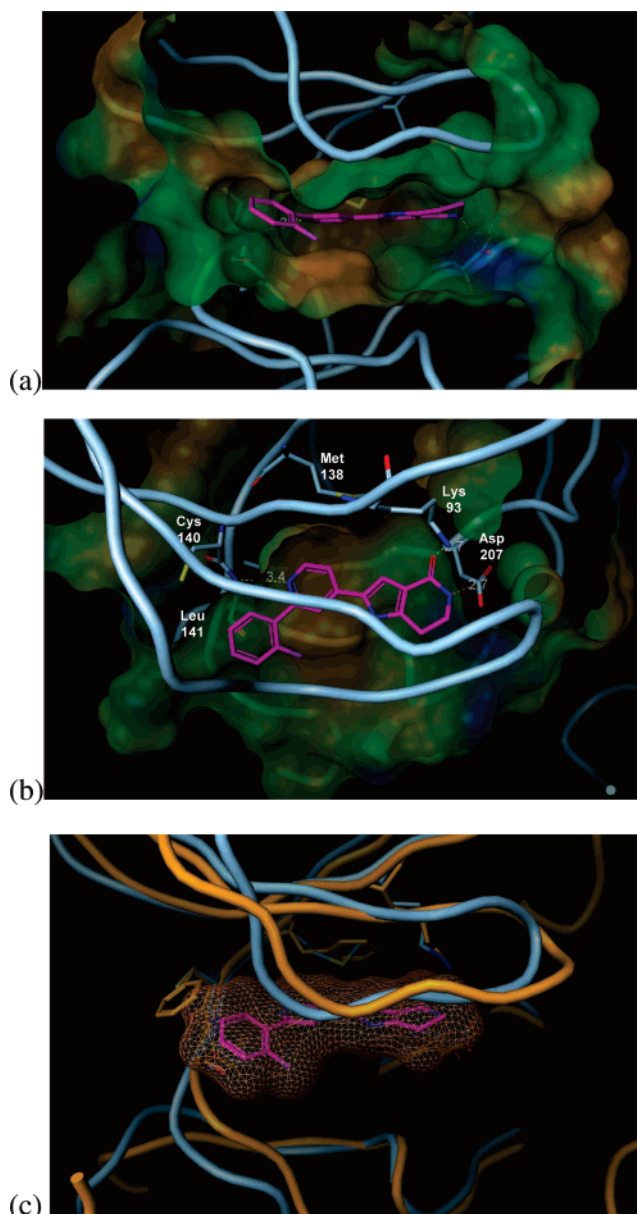


Figure 1. Crystal structure of MK-2 with compound **23**. (a) Edge view showing the MK-2 binding pocket with compound **23**. (b) Top view showing H-bonding network of **23** with Leu141, Lys93, and Asp207 in the MK-2 binding pocket. (c) Overlay of compound **23** bound to MK-2 (gray) and the ATP binding site of CDK2 (orange). In Figure 1a,b, the molecular surface of MK-2 is color-coded by hydrophobicity, with brown representing the most hydrophobic region of the protein and blue indicating the most hydrophilic region.

While this would explain the high binding affinity of compound **23** for MK-3, which also contains a cysteine at this position, it is unclear why this compound is also a good inhibitor of PRAK, which contains a methionine at the corresponding position. One explanation is that the methionine side chain of PRAK could adopt an alternate rotamer conformation that would result in a similar pocket in PRAK as that observed in the MK-2 structure.

In addition, the hinge region is shorter in many kinases, such as cyclin-dependent kinase family, relative to MK-2. Consequently, MK-2 has a larger pocket at the hinge region compared to CDK2, which is exploited by the large substituent from the 2-position of the pyridyl ring. The combination of a large amino acid side chain (phenylalanine) at the position corresponding to Cys140 of MK-2 and one amino acid deletion in the hinge region in CDK2 results in a crowded and smaller binding pocket.

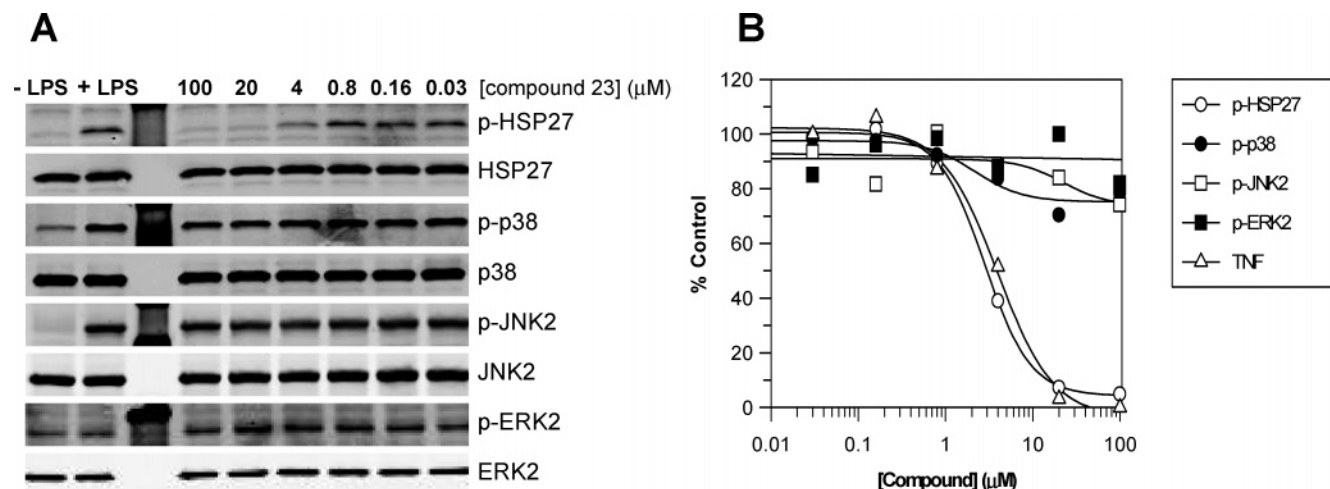


Figure 2. Western Blot analysis of MAPK signaling in U937 cells treated with MK-2 inhibitor **23**.

This smaller pocket in the hinge region of CDK2 precludes the binding of the terminal aryl group of compound **23**. This observation presents a general strategy for the design of specific inhibitors for MK-2.

In Vitro Cellular Potency and Selectivity. MK-2 inhibitor compounds were tested for activity in a U937 cellular TNF α production assay,¹⁷ and the results for selected analogs are summarized in Tables 1 and 2. As can be seen, many of these compounds are active in suppressing cellular production of TNF α , albeit with low micromolar potencies. Unfortunately, there is very little correlation between increased MK-2 potency and potency in the U937 cell assay. For example, the phenyl analog **9** is 66 nM in the enzyme assay and 1.4 μM in the cell assay, while the 3-quinoline derivative is about 8-fold more potent (8 nM) in the enzyme assay but only 4.4 μM in the cell.

Sub-optimal physical properties may contribute to the attenuated potencies of these inhibitors in the cellular assay. Many of the compounds have low aqueous solubilities. For example, quinoline analog **16** has an aqueous solubility of <0.4 μM . Some compounds have higher solubilities. For example, 2-fluorophenyl analog **23** has an aqueous solubility of 160 μM . The improved solubility of **23** may be related to the decreased planarity of the compound due to the slightly larger fluorine atom in the ortho position. Unfortunately, improving solubility by twisting the two aromatic groups from planarity often leads to weaker MK-2 potency (vide supra). When compared to the unsubstituted phenyl analog, the 2-fluorophenyl analog is approximately 2-fold less potent, with an IC₅₀ value of 0.126 μM . While this difference may not be statistically significant and within the error of the assay, it does follow the general trend that ortho-substitution is detrimental to enzyme potency. The 3- and 4-fluoro-substituted analogs **24** and **25** have solubilities of 130 and 20 μM , respectively, and have improved potencies for the recombinant enzyme (0.034 μM and 0.05 μM , respectively), but do not show markedly improved potency in the cellular assay (3.4 μM and 2.4 μM) when compared to **23**. This suggests that solubility alone cannot account for the attenuation in potency observed in the U937 cell for this series. Analog **23** has moderate to high permeability, as judged by CACO-2 (A-B = 9.45×10^{-6} cm/sec), and also has reasonably low rat plasma protein binding (92%). Protein binding of **23** in the media used in the cell assay containing 10% fetal calf serum was determined to be 31%.

Lack of correlation between isolated biochemical assays for kinases and cell-based assays are well documented, and it has been suggested that unfavorable competition with cellular ATP

levels may be a contributing factor.^{18,19} The source of the discrepancy between the enzyme and the cell potencies may be explained by an examination of the affinity of MK-2 for ATP. The measured in vitro K_m value of ATP for MK-2 is 30 μM . Because the inhibitors described are ATP competitive and ATP concentrations in the cell are 1–5 mM, one can use the Cheng–Prusoff equation²⁰ to calculate the theoretical shift in potencies from the enzyme assay to cell assay due to increased ATP concentrations. For MK-2, a shift of approximately 33-fold can be expected. Analog **23**, which has a moderate to high permeability, 69% unbound fraction in cell media, and high solubility, has a cell to enzyme ratio of 38, which is nearing this theoretical minimum based on differences in ATP concentrations in the assays. Deficiencies in physical properties that limit cell permeability or free drug concentration would be expected to exacerbate this discrepancy even further. We therefore conclude that unfavorable ATP competition is the most likely source of the discrepancy between enzyme and cell potencies.

Because the compounds described appear to be inactive against other kinases in signal transduction pathways known to affect the production of TNF α , but there is a shift in observed potency between enzyme and cell assays, we sought to determine whether the observed activity in the cell assay was solely due to inhibition of MK-2, or possibly a combination of pathways and mechanisms. We sought to demonstrate that blockade of MK-2 activity in a cell-based system correlated directly with inhibition of TNF α production. In Western blot analysis of LPS-stimulated U937 cells treated with various concentrations of compound **23**, we see dose-dependent inhibition of phospho-Ser78 on HSP27, a site shown to be specifically phosphorylated by MK-2²¹ (Figure 2A). The ratio of phospho-HSP27 to total HSP27 protein was quantified from the Western blot and expressed as percent control of the phospho levels detected after 30 min of LPS stimulation in the absence or presence of compound **23** (Figure 2B). Inhibition of HSP27 phosphorylation at 30 min correlated directly with TNF α inhibition measured at 4 h, with an IC₅₀ value of approximately 4 μM . Furthermore, compound **23** failed to inhibit upstream of MK-2 or within the JNK or ERK MAPK pathways, as measured by the lack of cellular inhibition of phospho-p38, phospho-JNK2, and phospho-ERK2, respectively. Because HSP27 phosphorylation and TNF α production are attenuated at roughly the same inhibitor concentrations and given the evidence linking MK-2 to TNF α production, it is reasonable to conclude that the activity in the cellular assay is the result of MK-2 inhibition.

Table 4. Efficacy of MK-2 Inhibitors an In Vivo Acute Model of Inflammation (rLPS)

cmpd	R	TNF α ^a (% inhibition)		[compound] ^b (μ g/mL)	
		2.5 h	3.5 h	2.5 h	3.5 h
9	Ph	44	<0.1	4.54	blq ^c
16	3-quinoliny	20	<0.1	blq	blq
22	4-Cl-Ph	38	<0.1	2.18	blq
29	4-MeO-Ph	<0.1	<0.1	blq	blq
23	2-F-Ph	73	87	3.87	3.13
24	3-F-Ph	55	83	nd ^d	5.80
25	4-F-Ph	57	49	nd	nd

^a Percent inhibition of TNF α production relative to control, 1.5 h after LPS challenge. Compounds were dosed orally at 20 mpk, 1 or 2 h prior to LPS challenge. ^b Compound concentrations in the plasma samples for TNF α levels were measured by LC-MS and correspond to 2.5 and 3.5 h after compound dosing. ^c blq = below limits of quantitation. ^d nd = not determined.

In Vivo Efficacy. Analogs with potencies less than 5 μ M in the cellular assay were tested in vivo. It was found that a number of the compounds tested were orally active in an acute model of inflammation, the rat LPS (rLPS) model.¹⁷ The results for a select group of analogs are shown in Table 4. While many potent MK-2 inhibitors had little or no oral activity in the rLPS assay, the fluorophenyl analogs (**23**–**25**) were found to be efficacious, presumably due to improved physical and pharmacokinetic properties. For example, analogs **9** and **22** showed low to moderate activity in the rLPS model at 20 mpk 1 h prior to LPS challenge with measurable levels of compound in the plasma. However, if dosed 2 h prior to the LPS challenge, no TNF α inhibition was observed and plasma compound concentrations were undetectable at 3.5 h, presumably due to high clearance or poor bioavailability of the compounds. Compounds **23** and **24**, on the other hand, inhibited >80% of TNF α production when dosed 2 h prior to LPS challenge, with good levels of compound detected in the plasma, most likely due to reduced clearance or other improved pharmacokinetic properties. In addition to potent TNF α inhibition, compound **23** has many desirable drug-like properties that will be explored in a forthcoming pharmacology publication.

In conclusion, we have prepared a set of potent small molecule inhibitors selective for MK-2 kinase. These compounds were found to be effective in reducing TNF α production in both U937 cells and in vivo. These results demonstrate that selective, small molecule MK-2 inhibitors have the potential to be effective treatments for RA and other inflammatory diseases mediated by TNF α .

Experimental Section

Chemistry. General Methods. All reagents were purchased from commercial sources and were used without further purification. Solvents were of analytical or anhydrous grade (Sigma-Aldrich). Reactions were monitored by HPLC. Reverse phase preparative HPLC was performed using a Gilson preparative HPLC system. ¹H NMR spectra were recorded on a Varian Unity Innova 400 instrument. Chemical shifts (δ) are reported in ppm downfield from solvent references. Mass spectra were obtained on a Finnigan LCQ Duo LCMS ion trap electrospray ionization (ESI) mass spectrometer, a PerSeptive Biosystems Mariner TOF HPLC-MS (ESI), or a Waters ZQ mass spectrometer (ESI). Elemental analyses were performed by Atlantic Microlabs, Norcross, GA, and are within $\pm 0.4\%$ of theoretical values.

2-Bromo-1-(2-chloropyridin-4-yl)ethanone Hydrobromide (4). 4-Acetyl-2-chloropyridine (**3**)¹⁵ was dissolved in glacial acetic acid (100 mL) and treated with bromine (1.26 mL, 24.6 mmol), followed by HBr/AcOH (30% w/v, 4.4 mL, 22.3 mmol). After 15 min of stirring, a precipitate formed, and the reaction was complete after 2–3 h. The reaction mixture was diluted with ethyl ether (100 mL),

and the solid was collected by filtration. The solid was washed with ethyl ether and dried under vacuum to give **4** (6.51 g, 93%) as a yellow solid. ¹H NMR (400 MHz, DMSO-*d*₆) δ 8.62 (d, 1H), 7.96 (s, 1H), 7.83 (d, 1H), 4.99 (s, 2H). MS *m/z* (M + H): 234, 236.

2,4-Dioxopiperidine (6). Sodium 3-(methoxycarbonyl)-4-oxo-1,4,5,6-tetrahydropyridin-2-olate (Degussa; 50 g, 259 mmol) was partitioned between 2 *N* aqueous hydrogen chloride and dichloromethane. The aqueous layer was extracted two additional times with dichloromethane. The organic extracts were dried over sodium sulfate, filtered, and evaporated. The residue was suspended in acetonitrile (500 mL) and water (100 mL) and heated to reflux for 3 h. The reaction mixture was cooled and evaporated. The residue was recrystallized from 1:1 ethyl acetate/hexane to provide **6** (19.5 g, 67%) as a white solid. ¹H NMR (400 MHz, CDCl₃) δ 7.05 (s, 1H), 3.58 (td, 2H), 3.34 (s, 2H), 2.64 (t, 2H). MS *m/z* (M + H): 114.

2-(2-Chloropyridin-4-yl)-1,5,6,7-tetrahydro-4H-pyrrolo[3,2-*c*]pyridin-4-one (6a). Bromoketone **4** (6.5 g, 20.6 mmol) was combined in absolute ethanol (65 mL) with ammonium acetate (6.35 g, 82.4 mmol) and dioxopiperidine **6** (2.57 g, 22.7 mmol). After 30 min, the mixture was diluted with water (130 mL) and the mixture was filtered. The resulting solid was washed with water and ethyl ether and dried under vacuum to give **7** (3.15 g, 62%) as a white solid. ¹H NMR (400 MHz, DMSO-*d*₆) δ 12.00 (s, 1H), 8.27 (d, 1H), 7.73 (s, 1H), 7.63 (d, 1H), 7.12 (s, 1H), 7.08 (s, 1H), 3.40 (td, 2H), 2.83 (t, 2H). MS *m/z* (M + H): 248.

2-Pyridin-4-yl-1,5,6,7-tetrahydro-4H-pyrrolo[3,2-*c*]pyridin-4-one Trifluoroacetate (8). A mixture of 4-(bromocetyl)pyridine hydrobromide (250 mg, 0.89 mmol), dioxopiperidine **6** (151 mg, 1.33 mmol, 1.5 equiv), and ammonium acetate (411 mg, 5.34 mmol, 4.0 equiv) in ethanol (3.0 mL) was stirred at room temperature for 1 h. The reaction mixture was purified by preparative reverse phase HPLC to give **8** (207 mg, 0.63 mmol, 71%). ¹H NMR (400 MHz, DMSO-*d*₆) δ ppm 12.82 (s, 1H), 8.66 (d, *J* = 7.0 Hz, 2H), 8.16 (d, *J* = 7.0 Hz, 2H), 7.52 (d, *J* = 2.4 Hz, 1H), 7.26 (s, 1H), 3.37–3.43 (m, 3H), 2.89 (t, *J* = 6.8 Hz, 2H). HRMS calcd for C₁₂H₁₂N₃O (MH⁺), 214.0975; found, 214.0949. Anal. (C₁₂H₁₁N₃O·CF₃CO₂H·0.2H₂O) C, H, N.

General Procedure for the Suzuki Coupling of Chloropyridine 6a with Aryl Boronic Acids. A suspension of chloropyridine **7** (1.0 equiv) in dimethylformamide (2.0 mL/100 mg **7**) was treated with an aryl boronic acid (1.5 equiv) and 2.0 M aqueous cesium carbonate (3.0 equiv). The reaction was purged with nitrogen and then tetrakis(triphenylphosphine)palladium (0.05 equiv) was added. The reaction was then heated to 80 °C for 8 to 16 h and then cooled to room temperature. The reaction mixture was acidified with trifluoroacetic acid and purified by preparative reverse phase HPLC (acetonitrile/water/0.05% trifluoroacetic acid). The desired fractions were lyophilized or concentrated under a stream of nitrogen to give the product. Compounds **9**–**35** were obtained in this manner.

2-(2-Phenylpyridin-4-yl)-1,5,6,7-tetrahydro-4H-pyrrolo[3,2-*c*]pyridin-4-one Trifluoroacetate (9): Yellow solid, 208 mg, 85%. ¹H NMR (400 MHz, DMSO-*d*₆) δ 12.34 (s, 1H), 8.63 (d, *J* = 5.9 Hz, 1H), 8.36 (s, 1H), 8.08 (dd, *J* = 7.6, 1.8 Hz, 2H), 7.86 (d, *J* = 5.7 Hz, 1H), 7.64–7.56 (m, 3H), 7.48 (s, 1H), 7.20 (s, 1H), 3.43 (t, *J* = 6.7 Hz, 2H), 2.91 (t, *J* = 6.8 Hz, 2H). HRMS calcd for C₁₈H₁₆N₃O (MH⁺), 290.1288; found, 290.1319. Anal. (C₁₈H₁₅N₃O·CF₃CO₂H·H₂O) C, H, N.

2-(2,4'-Bipyridin-4-yl)-1,5,6,7-tetrahydro-4H-pyrrolo[3,2-*c*]pyridin-4-one Trifluoroacetate (10): Yellow solid, 18 mg, 31%. ¹H NMR (400 MHz, DMSO-*d*₆) δ ppm 12.05 (s, 1H), 8.84–8.92 (m, 2H), 8.67 (d, *J* = 5.4 Hz, 1H), 8.50 (d, *J* = 1.1 Hz, 1H), 8.44 (d, *J* = 6.2 Hz, 2H), 7.74 (dd, *J* = 5.2, 1.7 Hz, 1H), 7.31 (d, *J* = 2.7 Hz, 1H), 7.07 (s, 1H), 3.41 (td, *J* = 6.8, 1.2 Hz, 2H), 2.86 (t, *J* = 6.8 Hz, 2H). HRMS calcd for C₁₇H₁₅N₄O (MH⁺), 291.1240; found, 291.1240. Anal. (C₁₇H₁₄N₄O·2.6CF₃CO₂H) C, H, N.

2-(2,3'-Bipyridin-4-yl)-1,5,6,7-tetrahydro-4H-pyrrolo[3,2-*c*]pyridin-4-one Trifluoroacetate (11): Yellow solid, 169 mg, 90%. ¹H NMR (400 MHz, DMSO-*d*₆) δ ppm 12.13 (s, 1H), 9.37 (s, 1H), 8.79 (d, *J* = 4.6 Hz, 1H), 8.73 (d, *J* = 8.3 Hz, 1H), 8.65 (d, *J* =

5.6 Hz, 1H), 8.41 (d, $J = 1.1$ Hz, 1H), 7.80 (dd, $J = 8.1, 5.1$ Hz, 1H), 7.76 (dd, $J = 5.5, 1.5$ Hz, 1H), 7.36 (d, $J = 2.4$ Hz, 1H), 7.12 (s, 1H), 3.41 (t, $J = 6.7$ Hz, 2H), 2.87 (t, $J = 6.8$ Hz, 2H). HRMS calcd for $C_{17}H_{15}N_4O$ (MH^+), 291.1240; found, 291.1219. Anal. ($C_{17}H_{14}N_4O \cdot 2CF_3CO_2H \cdot 0.8H_2O$) C, H, N.

2-(2-Pyrimidin-5-ylpyridin-4-yl)-1,5,6,7-tetrahydro-4H-pyrrolo[3,2-c]pyridin-4-one Trifluoroacetate (12): Yellow solid, 67 mg, 27%. 1H NMR (300 MHz, DMSO- d_6) δ 12.03 (s, 1H), 9.49 (s, 2H), 9.27 (s, 1H), 8.65 (d, $J = 5.4$ Hz, 1H), 8.40 (s, 1H), 7.71 (dd, $J = 5.4, 1.6$ Hz, 1H), 7.31 (d, $J = 2.2$ Hz, 1H), 7.10 (s, 1H), 3.42 (t, $J = 6.7$ Hz, 2H), 2.88 (t, $J = 6.8$ Hz, 2H). HRMS calcd for $C_{16}H_{14}N_5O$ (MH^+), 292.1193; found, 292.1179. Anal. ($C_{16}H_{13}N_5O \cdot CF_3CO_2H$) C, H, N.

2-(2-Thien-3-ylpyridin-4-yl)-1,5,6,7-tetrahydro-4H-pyrrolo[3,2-c]pyridin-4-one Trifluoroacetate (13): Yellow solid, 280 mg, 57%. 1H NMR (300 MHz, DMSO- d_6) δ 12.33 (s, 1H), 8.56 (d, $J = 6.0$ Hz, 1H), 8.45 (s, 1H), 8.37 (s, 1H), 7.89 (d, $J = 5.0$ Hz, 1H), 7.80 (m, 2H), 7.54 (s, 1H), 7.21 (s, 1H), 3.44 (m, 2H), 2.91 (t, $J = 6.7$ Hz, 2H). HRMS calcd for $C_{16}H_{13}N_3OS$ (MH^+), 296.0852; found, 296.0869. Anal. ($C_{16}H_{13}N_3OS \cdot CF_3CO_2H \cdot 1.4H_2O$) C, H, N.

2-[2-(2-Naphthyl)pyridin-4-yl]-1,5,6,7-tetrahydro-4H-pyrrolo[3,2-c]pyridin-4-one Trifluoroacetate (14): Yellow solid, 22 mg, 32%. 1H NMR (400 MHz, DMSO- d_6) δ ppm 12.28 (s, 1H), 8.68 (d, $J = 1.6$ Hz, 1H), 8.65 (d, $J = 5.6$ Hz, 1H), 8.48 (s, 1H), 8.21 (dd, $J = 8.6, 1.9$ Hz, 1H), 8.11 (d, $J = 8.6$ Hz, 1H), 8.05 (dd, $J = 6.3, 3.6$ Hz, 1H), 8.00 (dd, $J = 6.2, 3.5$ Hz, 1H), 7.58–7.64 (m, 2H), 7.44–7.48 (m, 1H), 7.16 (s, 1H), 3.42 (td, $J = 6.7, 1.6$ Hz, 2H), 2.90 (t, $J = 6.8$ Hz, 2H). HRMS calcd for $C_{22}H_{18}N_3O$ (MH^+), 340.1444; found, 340.1417. Anal. ($C_{22}H_{17}N_3O \cdot 1.3CF_3CO_2H \cdot 0.5H_2O$) C, H, N.

2-[2-(1-Benzothien-2-yl)pyridin-4-yl]-1,5,6,7-tetrahydro-4H-pyrrolo[3,2-c]pyridin-4-one Trifluoroacetate (15): Yellow solid, 139 mg, 38%. 1H NMR (300 MHz, DMSO- d_6) δ ppm 12.07 (s, 1H), 8.52 (d, $J = 5.4$ Hz, 1H), 8.43 (d, $J = 1.0$ Hz, 1H), 8.28 (s, 1H), 7.98–8.08 (m, 1H), 7.85–7.97 (m, 1H), 7.62 (dd, $J = 5.4, 1.8$ Hz, 1H), 7.37–7.49 (m, 2H), 7.28 (d, $J = 2.4$ Hz, 1H), 7.12 (br s, 1H), 3.45 (t, $J = 6.7$ Hz, 2H), 2.91 (t, $J = 6.8$ Hz, 2H). HRMS calcd for $C_{20}H_{16}N_3OS$ (MH^+), 346.1009; found, 346.1043. Anal. ($C_{20}H_{15}N_3OS \cdot CF_3CO_2H \cdot 0.3H_2O$) C, H, N.

2-(2-Quinolin-3-ylpyridin-4-yl)-1,5,6,7-tetrahydro-4H-pyrrolo[3,2-c]pyridin-4-one (16): Yellow solid, 51 mg, 75%. 1H NMR (300 MHz, DMSO- d_6) δ ppm 12.06 (s, 1H), 9.72 (d, $J = 2.2$ Hz, 1H), 9.12 (d, $J = 2.0$ Hz, 1H), 8.68 (d, $J = 5.2$ Hz, 1H), 8.49 (s, 1H), 8.12 (t, $J = 7.9$ Hz, 2H), 7.84 (ddd, $J = 8.5, 6.8, 1.6$ Hz, 1H), 7.64–7.75 (m, 2H), 7.29 (d, $J = 2.4$ Hz, 1H), 7.10 (br s, 1H), 3.46 (t, $J = 6.9$ Hz, 2H), 2.92 (t, $J = 7.0$ Hz, 2H). HRMS calcd for $C_{21}H_{17}N_4O$ (MH^+), 341.1397; found, 341.1352. Anal. ($C_{21}H_{16}N_4O \cdot 2.8CF_3CO_2H$) C, H, N.

2-[2-(2-Hydroxyphenyl)pyridin-4-yl]-1,5,6,7-tetrahydro-4H-pyrrolo[3,2-c]pyridin-4-one Trifluoroacetate (17): Yellow solid, 165 mg, 67%. 1H NMR (300 MHz, DMSO- d_6) δ 12.31 (s, 1H), 8.55 (d, $J = 6.0$ Hz, 1H), 8.37 (s, 1H), 7.95 (d, $J = 8.1$ Hz, 1H), 7.85 (d, $J = 5.8$ Hz, 1H), 7.47–7.35 (m, 2H), 7.19 (s, 1H), 7.04–6.96 (m, 2H), 3.43 (t, $J = 6.2$ Hz, 2H), 2.91 (t, $J = 6.6$ Hz, 2H). HRMS calcd for $C_{18}H_{15}N_3O_2$ (MH^+), 306.1237; found, 306.1250. Anal. ($C_{18}H_{15}N_3O_2 \cdot CF_3CO_2H \cdot 2.3H_2O$) C, H, N.

2-[2-(3-Hydroxyphenyl)pyridin-4-yl]-1,5,6,7-tetrahydro-4H-pyrrolo[3,2-c]pyridin-4-one Trifluoroacetate (18): 1H NMR (300 MHz, DMSO- d_6) δ 12.35 (s, 1H), 8.59 (d, $J = 6.0$ Hz, 1H), 8.31 (s, 1H), 7.87 (d, $J = 5.6$ Hz, 1H), 7.43 (m, 4H), 7.20 (s, 1H), 6.99 (d, $J = 7.8$ Hz, 2H), 3.43 (m, 2H), 2.90 (t, $J = 6.6$ Hz, 2H). HRMS calcd for $C_{18}H_{15}N_3O_2$ (MH^+), 306.1237; found, 306.1224. Anal. ($C_{18}H_{13}N_3O_2 \cdot CF_3CO_2H \cdot 2H_2O$) C, H, N.

2-[2-(4-Hydroxyphenyl)pyridin-4-yl]-1,5,6,7-tetrahydro-4H-pyrrolo[3,2-c]pyridin-4-one (19): Yellow solid, 109 mg, 59%. 1H NMR (300 MHz, DMSO- d_6) δ 12.42 (s, 1H), 8.54 (d, $J = 6.0$ Hz, 1H), 8.31 (s, 1H), 7.93 (d, $J = 8.6$ Hz, 2H), 7.85 (d, $J = 5.8$ Hz, 1H), 7.54 (s, 1H), 7.23 (s, 1H), 6.98 (d, $J = 8.6$ Hz, 2H), 3.43 (m,

2H), 2.91 (t, $J = 6.4$ Hz, 2H). HRMS calcd for $C_{18}H_{15}N_3O_2$ (MH^+), 306.1237; found, 306.1219. Anal. ($C_{18}H_{15}N_3O_2 \cdot CF_3CO_2H \cdot 1.9H_2O$) C, H, N.

2-[2-(2-Chlorophenyl)pyridin-4-yl]-1,5,6,7-tetrahydro-4H-pyrrolo[3,2-c]pyridin-4-one Trifluoroacetate (20): Yellow solid, 107 mg, 40%. 1H NMR (400 MHz, DMSO- d_6) δ ppm 12.24 (s, 1H), 8.68 (d, $J = 5.9$ Hz, 1H), 8.05 (s, 1H), 7.90 (d, $J = 5.4$ Hz, 1H), 7.64–7.71 (m, 2H), 7.49–7.62 (m, 2H), 7.35 (s, 1H), 7.19 (s, 1H), 3.41 (td, $J = 6.7, 2.4$ Hz, 2H), 2.87 (t, $J = 6.8$ Hz, 2H). HRMS calcd for $C_{18}H_{15}ClN_3O$ (MH^+), 324.0898; found, 324.0892. Anal. ($C_{18}H_{14}ClN_3O \cdot CF_3CO_2H \cdot 2H_2O$) C, H, N.

2-[2-(3-Chlorophenyl)pyridin-4-yl]-1,5,6,7-tetrahydro-4H-pyrrolo[3,2-c]pyridin-4-one Trifluoroacetate (21): Yellow solid, 31 mg, 48%. 1H NMR (400 MHz, DMSO- d_6) δ ppm 12.18 (s, 1H), 8.60 (d, $J = 5.6$ Hz, 2H), 8.33 (s, 1H), 8.17 (s, 1H), 8.07 (t, $J = 3.6$ Hz, 1H), 7.76 (d, $J = 5.4$ Hz, 1H), 7.58 (d, $J = 4.8$ Hz, 1H), 7.39 (d, $J = 1.1$ Hz, 1H), 7.13 (s, 1H), 3.41 (t, $J = 6.7$ Hz, 2H), 2.88 (t, $J = 6.7$ Hz, 2H). HRMS calcd for $C_{18}H_{15}ClN_3O$ (MH^+), 324.0898; found, 324.0886. Anal. ($C_{18}H_{14}ClN_3O \cdot 1.3CF_3CO_2H \cdot 0.4H_2O$) C, H, N.

2-[2-(4-Chlorophenyl)pyridin-4-yl]-1,5,6,7-tetrahydro-4H-pyrrolo[3,2-c]pyridin-4-one Trifluoroacetate (22): Yellow solid, 218 mg, 80%. 1H NMR (400 MHz, DMSO- d_6) δ ppm 12.18 (s, 1H), 8.58 (d, $J = 5.6$ Hz, 1H), 8.30 (d, $J = 1.3$ Hz, 1H), 8.05–8.17 (m, 2H), 7.74 (d, $J = 5.4$ Hz, 1H), 7.58–7.65 (m, 2H), 7.36 (s, 1H), 7.13 (s, 1H), 3.41 (t, $J = 6.4$ Hz, 2H), 2.87 (t, $J = 6.8$ Hz, 2H). HRMS calcd for $C_{18}H_{15}ClN_3O$ (MH^+), 324.0898; found, 324.0897. Anal. ($C_{18}H_{14}ClN_3O \cdot CF_3CO_2H \cdot H_2O$) C, H, N.

2-[2-(2-Fluorophenyl)pyridin-4-yl]-1,5,6,7-tetrahydro-4H-pyrrolo[3,2-c]pyridin-4-one Trifluoroacetate (23): Yellow solid, 168 mg, 70%. 1H NMR (400 MHz, DMSO- d_6) δ 12.25 (s, 1H), 8.67 (d, $J = 5.7$ Hz, 1H), 8.13 (s, 1H), 7.88–7.84 (m, 2H), 7.63–7.57 (m, 1H), 7.46–7.38 (m, 2H), 7.31 (s, 1H), 7.17 (s, 1H), 3.42 (t, $J = 6.7$ Hz, 2H), 2.88 (t, $J = 6.6$ Hz, 2H). HRMS calcd for $C_{18}H_{15}FN_3O$ (MH^+), 308.1194; found, 308.1224. Anal. ($C_{18}H_{14}FN_3O \cdot CF_3CO_2H \cdot 1.2H_2O$) C, H, N.

2-[2-(3-Fluorophenyl)pyridin-4-yl]-1,5,6,7-tetrahydro-4H-pyrrolo[3,2-c]pyridin-4-one Trifluoroacetate (24): Yellow solid, 127 mg, 51%. 1H NMR (400 MHz, DMSO- d_6) δ 12.19 (s, 1H), 8.62 (d, $J = 5.6$ Hz, 1H), 8.35 (s, 1H), 7.99–7.94 (m, 2H), 7.78 (d, $J = 4.8$ Hz, 1H), 7.63 (td, $J = 8.1, 6.4$ Hz, 1H), 7.40 (s, 1H), 7.35 (td, $J = 8.3, 2.2$ Hz, 1H), 7.16 (s, 1H), 3.43 (t, $J = 6.8$ Hz, 2H), 2.90 (t, $J = 6.8$ Hz, 2H). HRMS calcd for $C_{18}H_{15}FN_3O$ (MH^+), 308.1194; found, 308.1162. Anal. ($C_{18}H_{14}FN_3O \cdot CF_3CO_2H \cdot 1.4H_2O$) C, H, N.

2-[2-(4-Fluorophenyl)pyridin-4-yl]-1,5,6,7-tetrahydro-4H-pyrrolo[3,2-c]pyridin-4-one Trifluoroacetate (25): Yellow solid, 229 mg, 67%. 1H NMR (400 MHz, DMSO- d_6) δ ppm 12.18 (s, 1H), 8.58 (d, $J = 5.9$ Hz, 1H), 8.28 (s, 1H), 8.11–8.17 (m, 2H), 7.75 (d, $J = 5.1$ Hz, 1H), 7.35–7.45 (m, $J = 8.9, 8.9$ Hz, 3H), 7.13 (s, 1H), 3.38–3.44 (m, 2H), 2.87 (t, $J = 6.8$ Hz, 2H). HRMS calcd for $C_{18}H_{15}FN_3O$ (MH^+), 308.1194; found, 308.1155. Anal. ($C_{18}H_{14}FN_3O \cdot CF_3CO_2H \cdot 1.1H_2O$) C, H, N.

2-[2-[4-(Trifluoromethyl)phenyl]pyridin-4-yl]-1,5,6,7-tetrahydro-4H-pyrrolo[3,2-c]pyridin-4-one Trifluoroacetate (26): Yellow solid, 27 mg, 38%. 1H NMR (400 MHz, DMSO- d_6) δ ppm 12.11 (s, 1H), 8.61 (d, $J = 5.4$ Hz, 1H), 8.26–8.41 (m, 2H), 7.89 (d, $J = 8.3$ Hz, 2H), 7.72 (dd, $J = 5.6, 1.6$ Hz, 1H), 7.29 (d, $J = 2.4$ Hz, 1H), 7.09 (s, 1H), 3.41 (t, $J = 6.7$ Hz, 1H), 2.87 (t, $J = 6.8$ Hz, 1H). HRMS calcd for $C_{19}H_{15}N_3OF_3$ (MH^+), 358.1162; found, 358.1162. Anal. ($C_{19}H_{14}N_3OF_3 \cdot CF_3CO_2H \cdot H_2O$) C, H, N.

4-[4-(2-Oxo-4,5,6,7-tetrahydro-1H-pyrrolo[3,2-c]pyridin-2-yl)pyridin-2-yl]benzoxonitrile Trifluoroacetate (27): Yellow solid, 56 mg, 7%. 1H NMR (300 MHz, DMSO- d_6) δ ppm 12.12 (s, 1H), 8.65 (d, $J = 5.4$ Hz, 1H), 8.32–8.42 (m, 3H), 8.04 (d, $J = 8.7$ Hz, 2H), 7.74 (dd, $J = 5.4, 1.6$ Hz, 1H), 7.33 (d, $J = 2.2$ Hz, 1H), 7.13 (br s, 1H), 3.45 (t, $J = 6.6$ Hz, 2H), 2.90 (t, $J = 6.8$ Hz, 2H). HRMS calcd for $C_{19}H_{15}N_4O$ (MH^+), 315.1240; found, 315.1235. Anal. ($C_{19}H_{14}N_4O \cdot CF_3CO_2H \cdot 1.5H_2O$) C, H, N.

2-[2-(4-Acetylphenyl)pyridin-4-yl]-1,5,6,7-tetrahydro-4H-pyrrolo[3,2-c]pyridin-4-one Trifluoroacetate (28): Yellow solid, 15

mg, 22%. ¹H NMR (400 MHz, DMSO-*d*₆) δ 12.10 (s, 1H), 8.59 (d, *J* = 5.6 Hz, 1H), 8.33 (s, 1H), 8.26 (d, *J* = 8.4 Hz, 2H), 8.08 (d, *J* = 8.4 Hz, 2H), 7.69 (d, *J* = 4.8 Hz, 1H), 7.28 (s, 1H), 7.09 (s, 1H), 3.46–3.38 (m, 4H), 2.87 (t, *J* = 6.8 Hz, 2H), 2.62 (s, 3H). HRMS calcd for C₂₀H₁₈N₃O₂ (MH⁺), 332.1394; found, 332.1394. Anal. (C₂₀H₁₇N₃O₂·1.4CF₃CO₂H·0.9H₂O) C, H, N.

2-[2-(4-Methoxyphenyl)pyridin-4-yl]-1,5,6,7-tetrahydro-4H-pyrrolo[3,2-*c*]pyridin-4-one Trifluoroacetate (29): Yellow solid, 33 mg, 52%. ¹H NMR (400 MHz, DMSO-*d*₆) δ ppm 12.35 (s, 1H), 8.55 (d, *J* = 6.2 Hz, 1H), 8.32 (s, 1H), 7.98–8.07 (m, 2H), 7.83 (d, *J* = 5.6 Hz, 1H), 7.52 (s, 1H), 7.10–7.26 (m, 3H), 3.85 (s, 3H), 3.42 (td, *J* = 6.8, 2.1 Hz, 2H), 2.89 (t, *J* = 6.8 Hz, 2H). HRMS calcd for C₁₉H₁₈N₃O₂ (MH⁺), 320.1394; found, 320.1390. Anal. (C₁₉H₁₇N₃O₂·1.3CF₃CO₂H·H₂O) C, H, N.

2-[2-(4-Aminophenyl)pyridin-4-yl]-1,5,6,7-tetrahydro-4H-pyrrolo[3,2-*c*]pyridin-4-one Trifluoroacetate (30): Yellow solid, 140 mg, 76%. ¹H NMR (300 MHz, DMSO-*d*₆) δ 12.48 (s, 1H), 8.43 (d, *J* = 6.4 Hz, 1H), 8.30 (s, 1H), 7.82 (m, 3H), 7.61 (s, 3H), 7.26 (s, 1H), 6.75 (d, *J* = 8.6 Hz, 2H), 3.43 (m, 2H), 2.92 (t, *J* = 6.8 Hz, 2H). HRMS calcd for C₁₈H₁₆N₄O (MH⁺), 305.1397; found, 305.1385. Anal. (C₁₈H₁₆N₄O·1.2CF₃CO₂H·1.3H₂O) C, H, N.

4-[4-(4-Oxo-4,5,6,7-tetrahydro-1H-pyrrolo[3,2-*c*]pyridin-2-yl)pyridin-2-yl]benzoic Acid Trifluoroacetate (31): Yellow solid, 110 mg, 42%. ¹H NMR (300 MHz, DMSO-*d*₆) δ 12.25 (s, 1H), 8.64 (d, *J* = 5.4 Hz, 1H), 8.39 (s, 1H), 8.23 (d, *J* = 8.5 Hz, 2H), 8.10 (d, *J* = 8.3 Hz, 2H), 7.81 (d, *J* = 5.2 Hz, 1H), 7.40 (s, 1H), 7.16 (s, 1H), 3.43 (t, *J* = 6.1 Hz, 2H), 2.90 (t, *J* = 6.6 Hz, 2H). HRMS calcd for C₁₉H₁₅N₃O₃ (MH⁺), 334.1186; found, 334.1188. Anal. (C₁₉H₁₅N₃O₃·1.2CF₃CO₂H·1.6H₂O) C, H, N.

N-Cyclopropyl-4-[4-(4-oxo-4,5,6,7-tetrahydro-1H-pyrrolo[3,2-*c*]pyridin-2-yl)pyridin-2-yl]benzamide (32): Yellow solid, 230 mg, 76%. ¹H NMR (300 MHz, DMSO-*d*₆) δ 12.27 (s, 1H), 8.63 (d, *J* = 5.8 Hz, 1H), 8.59 (d, *J* = 4.2 Hz, 1H), 8.38 (s, 1H), 8.18 (d, *J* = 8.4 Hz, 2H), 7.99 (d, *J* = 8.5 Hz, 2H), 7.81 (d, *J* = 4.6 Hz, 1H), 7.43 (s, 1H), 7.17 (s, 1H), 3.43 (t, *J* = 6.7 Hz, 2H), 2.95–2.81 (m, 3H), 0.77–0.55 (m, 4H). HRMS calcd for C₂₂H₂₀N₄O₂ (MH⁺), 373.1659; found, 373.1638. Anal. (C₂₂H₂₀N₄O₂·CF₃CO₂H·1.6H₂O) C, H, N.

N-Cyclopentyl-4-[4-(4-oxo-4,5,6,7-tetrahydro-1H-pyrrolo[3,2-*c*]pyridin-2-yl)pyridin-2-yl]benzamide (33): Yellow solid, 210 mg, 65%. ¹H NMR (300 MHz, DMSO-*d*₆) δ 12.28 (s, 1H), 8.64 (d, *J* = 5.6 Hz, 1H), 8.46–8.36 (m, 2H), 8.19 (d, *J* = 8.5 Hz, 2H), 8.03 (d, *J* = 8.7 Hz, 2H), 7.85–7.74 (m, 1H), 7.44 (s, 1H), 7.17 (s, 1H), 4.33–4.18 (m, 1H), 3.43 (t, *J* = 6.7 Hz, 2H), 2.90 (t, *J* = 6.8 Hz, 2H), 1.98–1.47 (m, 8H). HRMS calcd for C₂₄H₂₄N₄O₂ (MH⁺), 401.1972; found, 401.1982. Anal. (C₂₄H₂₄N₄O₂·1.2CF₃CO₂H·0.6H₂O) C, H, N.

N-Cyclohexyl-4-[4-(4-oxo-4,5,6,7-tetrahydro-1H-pyrrolo[3,2-*c*]pyridin-2-yl)pyridin-2-yl]benzamide Trifluoroacetate (34): Yellow solid, 90 mg, 36%. ¹H NMR (300 MHz, DMSO-*d*₆) δ 12.19 (s, 1H), 8.57 (d, *J* = 5.8 Hz, 1H), 8.29 (m, 2H), 8.13 (d, *J* = 8.4 Hz, 2H), 7.96 (d, *J* = 8.4 Hz, 2H), 7.74 (s, 1H), 7.36 (s, 1H), 7.11 (s, 1H), 3.73 (m, 1H), 3.37 (t, *J* = 6.7 Hz, 2H), 2.84 (t, *J* = 6.8 Hz, 2H), 1.77 (m, 2H), 1.69 (m, 2H), 1.56 (m, 1H), 1.26 (m, 4H), 1.09 (m, 1H). HRMS calcd for C₂₅H₂₆N₄O₂ (MH⁺), 415.2129; found, 415.2156. Anal. (C₂₅H₂₆N₄O₂·CF₃CO₂H·2.1H₂O) C, H, N.

N-Benzyl-4-[4-(4-oxo-4,5,6,7-tetrahydro-1H-pyrrolo[3,2-*c*]pyridin-2-yl)pyridin-2-yl]benzamide Trifluoroacetate (35): Yellow solid, 240 mg, 70%. ¹H NMR (300 MHz, DMSO-*d*₆) δ 12.25 (s, 1H), 9.20 (t, *J* = 6.4 Hz, 1H), 8.63 (d, *J* = 5.6 Hz, 1H), 8.39 (s, 1H), 8.22 (d, *J* = 8.4 Hz, 2H), 8.08 (d, *J* = 8.4 Hz, 2H), 7.86–7.78 (m, 1H), 7.42 (s, 1H), 7.37–7.14 (m, 6H), 4.52 (m, 2H), 3.43 (t, *J* = 6.7 Hz, 2H), 2.90 (t, *J* = 6.8 Hz, 2H). HRMS calcd for C₂₆H₂₂N₄O₂ (MH⁺), 423.1816; found, 423.1811. Anal. (C₂₆H₂₂N₄O₂·CF₃CO₂H·H₂O) C, H, N.

4-(4-(4,5,6,7-Tetrahydro-4-oxo-1H-pyrrolo[3,2-*c*]pyridin-2-yl)pyridin-2-yl)-N-phenethylbenzamide (36). A solution of 4-[4-(4-oxo-4,5,6,7-tetrahydro-1H-pyrrolo[3,2-*c*]pyridin-2-yl)pyridin-2-yl]benzoic acid trifluoroacetate **31** (200 mg, 0.77 mmol), EDCl (164 mg, 0.86 mmol), and HOBt (116 mg, 0.86 mmol) in 4.0 mL of DMF was treated with phenethylamine (0.115 mL, 0.92 mmol)

followed by DIEA (0.38 mL, 2.3 mmol). Heated to 50 °C for 16 h, cooled, filtered through a syringe filter (0.2 micron), purified by reverse phase HPLC, and lyophilized to give the title compound as a yellow solid (118 mg, 0.27 mmol, 35%). ¹H NMR (300 MHz, DMSO-*d*₆) δ 12.25 (s, 1H), 8.72 (t, *J* = 5.6 Hz, 1H), 8.64 (d, *J* = 5.6 Hz, 1H), 8.39 (s, 1H), 8.20 (d, *J* = 8.4 Hz, 2H), 8.00 (d, *J* = 8.4 Hz, 2H), 7.80 (d, *J* = 5.6 Hz, 1H), 7.42 (s, 1H), 7.34–7.13 (m, 6H), 3.56–3.38 (m, 4H), 2.94–2.83 (m, 4H). HRMS calcd for C₂₇H₂₄N₄O₂ (MH⁺), 437.1972; found, 437.1991. Anal. (C₂₇H₂₄N₄O₂·CF₃CO₂H·0.7H₂O) C, H, N.

N-Benzyl-4-(4-(4,5,6,7-tetrahydro-4-oxo-1H-pyrrolo[3,2-*c*]pyridin-2-yl)pyridin-2-yl)-N-methylbenzamide (37). The title compound was prepared as described for compound **36** using *N*-methylbenzyl amine (0.12 mL, 0.92 mmol). The title compound was obtained as yellow solid (112 mg, 0.25 mmol, 32%). ¹H NMR (300 MHz, DMSO-*d*₆) δ 12.26 (s, 1H), 8.62 (s, 1H), 8.37 (s, 1H), 8.17 (m, 2H), 7.82 (s, 1H), 7.67 (m, 2H), 4.70 (br s, 1H), 4.51 (br s, 1H), 3.43 (t, *J* = 6.2 Hz, 1H), 2.91 (m, 5H). HRMS calcd for C₂₇H₂₄N₄O₂ (MH⁺), 437.1972; found, 437.1935. Anal. (C₂₇H₂₄N₄O₂·CF₃CO₂H·1.6H₂O) C, H, N.

Enzyme, U937 Cell, and Rat LPS Assays. The MK-2 enzyme assay, U937-TNFα cell, and rLPS-TNFα assays were performed as described previously.¹⁷ The MK-2 assay conditions were modified to include 15 nM MK-2 enzyme, 30 μM ATP (~*K*_m levels), and 200 μM HSP27 peptide (KKKALSRNLSVAA). Compound selectivity toward kinases was evaluated for inhibition of peptide phosphorylation using in-house recombinant enzymes and the anion exchange resin capture assay method as described.¹⁷ Specific selectivity assay conditions are described in the Supporting Information.

U937 Cell Signaling Studies. PMA-differentiated U937 cells were incubated with test compound in DMSO (1% final conc) for 1 h prior to stimulation with LPS (100 ng/mL final conc). After 30 min, media was removed and cells were solubilized at 8 million cells/mL using 2× SDS-PAGE sample buffer (Invitrogen). Boiled samples (5–10 μL/lane) were resolved on a 10–20% SDS-PAGE Tris-glycine gradient gel and transferred to a nitrocellulose membrane. The membrane was blocked for 1 h at 25 °C in Odyssey blocking buffer (OBB; LiCor Biosciences, Lincoln, NE) and then incubated overnight at 4 °C with primary antibody diluted in OBB/0.1% Tween 20 buffer. Primary antibodies and dilutions used were 1:750 rabbit anti-pT180/pY182 p38 (cell signaling #9211S), 1:1000 goat anti-p38 total (Santa Cruz #SC-535G), 1:2000 rabbit anti-pS78 HSP27 (in-house generated), 1:1000 goat anti-HSP27 total (Santa Cruz #SC1048), 1:1000 rabbit anti-pT182/pY185 JNK (Biosource #44-682G), 1:1000 goat anti-JNK2 total (Santa Cruz #SC-7345), 1:2000 rabbit anti-pT185/pY185 ERK (Biosource #44-680G), and 1:3000 mouse anti-ERK2 total (Santa Cruz #SC-1647). Membranes were washed 3 × 10 min with 25 mL Tris-buffered saline/0.1% Tween 20 (TBST) and then incubated for 1 h at 25 °C with secondary antibodies diluted 1:10 000 in OBB/0.1% Tween 20: donkey anti-rabbit IgG-fluor 700 (Rockland #611-730-127), donkey anti-goat IgG-IR dye 800 (Rockland #605-730-125), and donkey anti-mouse IgG-IR dye 800 (Rockland #610-732-124). Membranes were washed as above followed by a 25 mL PBS wash, and imaging was done on a LI-COR Odyssey Infrared Imaging System (LiCore Biosciences). Dye-labeled target bands were digitized and quantified, and IC₅₀'s were determined using Grafit (Erithacus Software Limited, Surrey, U.K.).

Crystallization of MAPKAP Kinase-2 (MK-2). Human MAPKAP kinase-2 (MK-2) spanning amino acids 45–371 was expressed in *E. coli* with an N-terminal hexa-histidine tag and purified by immobilized metal affinity chromatography, followed by ion exchange chromatography. Crystallization experiments of MK-2/inhibitor complex (5 mg/mL of protein along with 1 mM of compound **23** dissolved in DMSO) were set up at room temperature by hanging drop vapor diffusion against a well solution of 1.6–2.0 M sodium malonate, pH 5.4. Larger crystals with square-bipyramidal morphology were grown by microseeding into clear drops at lower precipitant concentrations. These crystals belong to face-centered cubic lattice and have the space group, *F*4132, with

lattice edges of 253.9 Å, with one molecule per asymmetric unit. Complete diffraction data was collected to 3.5 Å resolution at Advanced Photon Source IMCA CAT (sector 17). The structure was solved by difference Fourier methods using the coordinates of MK-2/AMP-PNP complex.¹⁶ Clear electron density was visible for the ligand at the ATP site. The ligand was included in the final rounds of refinement with final crystallographic *R*-factor 30.3% to 3.8 Å resolution. Coordinates for the complex of MK-2 with compound **23** have been deposited in the Protein Data Bank under PDB ID 2P3G.

Acknowledgment. We thank John E. Baldus and Ingrid P. Buchler for chemical synthesis contributions; Robert P. Compton, Jeffrey L. Hirsch, Heidi M. Morgan, and Matthew J. Saabye for enzymology support; Heidi R. Hope, Shelia C. Short, and Jian Zhang for cell assay and signaling studies; Richard M. Broadus for protein production; and Stephen J. Mnich, Sarah A. South, Mark A. Thiede, and Elizabeth G. Webb for in vivo model support. Use of the IMCA-CAT beamline 17-ID (or 17-BM) at the Advanced Photon Source was supported by the companies of the Industrial Macromolecular Crystallography Association through a contract with the Center for Advanced Radiation Sources at the University of Chicago. Use of the Advanced Photon Source was supported by the U.S. Department of Energy, Office of Science, Office of Basic Energy Sciences, under Contract No. W-31-109-Eng-38.

Supporting Information Available: Combustion analysis data, kinase selectivity assay protocols, CACO-2 assay protocols, ATP competition experiments, and K_m determinations. This material is available free of charge via the Internet at <http://pubs.acs.org>.

References

- Camussi, G.; Lupia, E. The future role of anti-tumor necrosis factor (TNF) products in the treatment of rheumatoid arthritis. *Drugs* **1998**, *55* (5), 613–620.
- Braun, J.; Sieper, J. Role of novel biological therapies in psoriatic arthritis: Effects on joints and skin. *BioDrugs* **2003**, *17* (3), 187–199.
- Jarvis, B.; Faulds, D. Etanercept: A review of its use in rheumatoid arthritis. *Drugs* **1999**, *57* (6), 945–966.
- Richard-Miceli, C.; Dougados, M. Tumour necrosis factor- α blockers in rheumatoid arthritis: Review of the clinical experience. *BioDrugs* **2001**, *15* (4), 251–259.
- Seymour, H. E.; Worsley, A.; Smith, J. M.; Thomas, S. H. L. Anti-TNF agents for rheumatoid arthritis. *Br. J. Clin. Pharmacol.* **2001**, *51* (3), 201–208.
- Adams, J. L.; Badger, A. M.; Kumar, S.; Lee, J. C. p38 MAP kinase: Molecular target for the inhibition of pro-inflammatory cytokines. *Prog. Med. Chem.* **2001**, *38*, 1–60.
- Lee, J. C.; Laydon, J. T.; McDonnell, P. C.; Gallagher, T. F.; Kumar, S.; Green, D.; McNulty, D.; Blumenthal, M. J.; Heyes, J. R.; Landvatter, S. W.; Strickler, J. E.; McLaughlin, M. M.; Siemens, I. R.; Fisher, S. M.; Livi, G. P.; White, J. R.; Adams, J. L.; Young, P. R. A protein kinase involved in the regulation of inflammatory cytokine biosynthesis. *Nature (London)* **1994**, *372* (6508), 739–746.
- Haddad, J. J. VX-745, Vertex Pharmaceuticals. *Curr. Opin. Invest. Drugs* **2001**, *2* (8), 1070–1076.
- Dambach, D. M. Potential adverse effects associated with inhibition of p38 α/β MAP kinases. *Curr. Top. Med. Chem.* **2005**, *5*, 929–939.
- Ding, C. Drug evaluation: VX-702, a MAP kinase inhibitor for rheumatoid arthritis and acute coronary syndrome. *Curr. Opin. Invest. Drugs* **2006**, *7*, 1020–1025.
- Kotlyarov, A.; Neininger, A.; Schubert, C.; Eckert, R.; Birchmeier, C.; Volk, H.-D.; Gaestel, M. MAPKAP kinase 2 is essential for LPS-induced TNF- α biosynthesis. *Nat. Cell Biol.* **1999**, *1* (2), 94–97.
- Winzen, R.; Kracht, M.; Ritter, B.; Wilhelm, A.; Chen, C.-Y. A.; Shyu, A.-B.; Muller, M.; Gaestel, M.; Resch, K.; Holtmann, H. The p38 MAP kinase pathway signals for cytokine-induced mRNA stabilization via MAP kinase-activated protein kinase 2 and an AU-rich region-targeted mechanism. *EMBO J.* **1999**, *18* (18), 4969–4980.
- Gaestel, M. MAPKAP kinases—MKs—two's company, three's a crowd. *Nat. Rev. Mol. Cell Biol.* **2006**, *7* (2), 120–130.
- Anderson, D. R.; Mahoney, M. W.; Phillion, D. P.; Rogers, T. E.; Meyers, M. J.; Poda, G.; Hegde, S. G.; Singh, K.; Reitz, D. B.; Wu, K. K.; Buchler, I. P.; Xie, J.; Vernier, W. F. Preparation of pyrrolopyridinones as mitogen activated protein kinase-activated protein kinase-2 inhibiting compounds. WO 2004/058762 A1, 2004.
- LaMattina, J. L. The synthesis of 2-amino-4-(4-imidazolyl)pyridines. *J. Heterocycl. Chem.* **1983**, *20* (3), 533–538.
- Kurumbail, R. G.; Pawlitz, J. P.; Stegeman, R. A.; Stallings, W. C.; Shieh, H. S.; Mourey, R. M.; Bolten, S. L.; Broadus, R. M. Crystalline structure of human MAPKAP kinase-2. Patent application WO2003076333 A2, 2003.
- Anderson, D. R.; Hegde, S.; Reinhard, E.; Gomez, L.; Vernier, W. F.; Lee, L.; Liu, S.; Sambandam, A.; Snider, P. A.; Masih, L. Aminocyanopyridine inhibitors of mitogen activated protein kinase-activated protein kinase 2 (MK-2). *Bioorg. Med. Chem. Lett.* **2005**, *15* (6), 1587–1590.
- Knight, Z. A.; Shokat, K. M. Features of selective kinase inhibitors. *Chem. Biol.* **2005**, *12*, 621–637.
- Swinney, D. C. Biochemical mechanisms of drug action: what does it take for success? *Nat. Rev. Drug Discovery* **2004**, *3*, 801–808.
- Cheng, Y.; Prusoff, W. H. Relationship between the inhibition constant (K_i) and the concentration of inhibitor which causes 50 per cent inhibition (IC_{50}) of an enzymatic reaction. *Biochem. Pharmacol.* **1973**, *22*, 3099–3108.
- Stokoe, D.; Engel, K.; Campbell, D. G.; Cohen, P.; Gaestel, M. Identification of MAPKAP kinase 2 as a major enzyme responsible for the phosphorylation of the small mammalian heat shock proteins. *FEBS Lett.* **1992**, *313*, 307–313.

JM0611004